ANNALS OF GEOPHYSICS, 67,1, SE110, doi:10.4401/ag-9072
OPEN ACCESS

Local Magnitude Scale and 1-D Velocity Model for Central Northern India

Deepak Kumar[*,1], Gaddale Suresh[2], Mukat Lal Sharma[1], Subhash Chandra Gupta[1]

(1) Department of Earthquake Engineering, Indian Institute of Technology, Roorkee-247667
(2) National Centre for Seismology, Ministry of Earth Sciences, Lodhi Road, New Delhi-110 003

Article history: received February 8, 2024; accepted May, 6, 2024

Abstract

Northern India's seismic monitoring has advanced significantly in the past with the establishment of a dense and well-distributed network of seismometers. This has greatly enhanced the ability to detect and analyze seismic events in the region and provided a high-quality dataset within the study region. We use the 20-year dataset of 413 earthquakes comprising 3,191 P-arrivals and 2,986 S-arrivals to develop a 1-D velocity model for the region. The dataset is meticulously curated based on the azimuthal gap, minimum station requirements, and root mean square travel-time residual. A collection of preliminary models taken from previous studies conducted in and around the central north Indian region is subjected to random perturbations and utilized in a coupled hypocenter and 1-D seismic velocity inversion. The model exhibiting a reduced travel time residual in comparison to its predecessors is adopted as the final 1-D velocity model. This final five layered model up to a depth of 100 km reveals a sediment thickness of 3.5 km with a P-wave velocity of 3.9 km/s and an upper crustal layer down to 20 km with a P-wave velocity of 6.01 km/s, and Moho depth of 43 km with P-wave and S-wave velocities at the Moho of 8.18 km/s and 4.71 km/s, respectively. Additionally, in defining the local magnitude scale (M_L) for Central Northern India, 166 earthquakes were analyzed, each with at least three synthetic Wood-Anderson amplitudes recorded, using a dataset comprised of 1404 maximum amplitudes of S- and Lg waves. This developed scale based on seismic wave amplitude (A), hypocentral distance (R), and a station correction term (S), is validated for earthquakes with magnitudes up to 4.6 (Mw) over hypocentral distances up to 1000 km.

Keywords: 1-D velocity model; Local magnitude scale (M_L); Northern India; Seismic monitoring Travel time residual

1. Introduction

The Central Northern India comprising Delhi and its surroundings, as delineated by India's seismic zoning map, is under Very High Risk Zone V (MSK IX or more), Zone IV High Risk Zone (MSK VIII), as per Bureau of Indian Standards ((IS-1893-Part-1-(2016), 2016). Geographically, it is positioned along the western boundary of the Ganga sedimentary basin and lies to the east of the Delhi-Hardwar Ridge (DHR). This region is known for its significant seismic activity, having been affected by earthquakes originating from both the Himalayas and peninsular India.

Prominent seismic events in and around area includes the 6.4-magnitude Uttarkashi earthquake on October 20, 1991, the 6.8-magnitude Chamoli earthquake on March 29, 1999, and earlier occurrences such as the 6.5-magnitude Delhi earthquake in 1720, the 6.8-magnitude Mathura earthquake in 1803, the 6.7-magnitude Bulandshahar earthquake in 1956, and the 4.8-magnitude Faridabad earthquake in 1960 [Singh et al., 2013]. The National Capital Region (NCR) witnessed a series of earthquakes commencing on April 12, 2020, with the first quake registering a magnitude of Mw 3.3. This seismic activity continued with several incidents, including quakes on May 10, 2020 (Mw: 3.3), May 29, 2020 (Mw: 4.0), and July 3, 2020 (Mw: 3.9). These events, predominantly felt within the NCR, caused considerable public alarm.

These seismic events were particularly experienced with significant strength within the NCR vicinity, prompting public worry and concern. Pandey et al. (2020) examined this seismic activity, encompassing the inversion of regional moment tensor and characterization of source spectrum analysis of the earthquakes. Furthermore, their research presented a thorough exploration of the ground movement linked to the event, delivering valuable insights into the behavior of the earthquake and its consequences on the surrounding region. The current study incorporates all of these event details.

Building on the seismic context of Central Northern India, it's essential to recognize the role of the Himalayan fault systems, which emerged from the collision between the Indian and Eurasian plates. These fault systems are a primary factor in the region's seismic vulnerability, as highlighted in studies by Chandra [1992], Sharma et al. [2003], and Sharma [2003]. The geological framework of Central Northern India is further complexified by an array of local tectonic structures. These include the Aravalli-Delhi Fold Belt (AFB), the Mahendragarh-Dehradun Fault (MDF), the

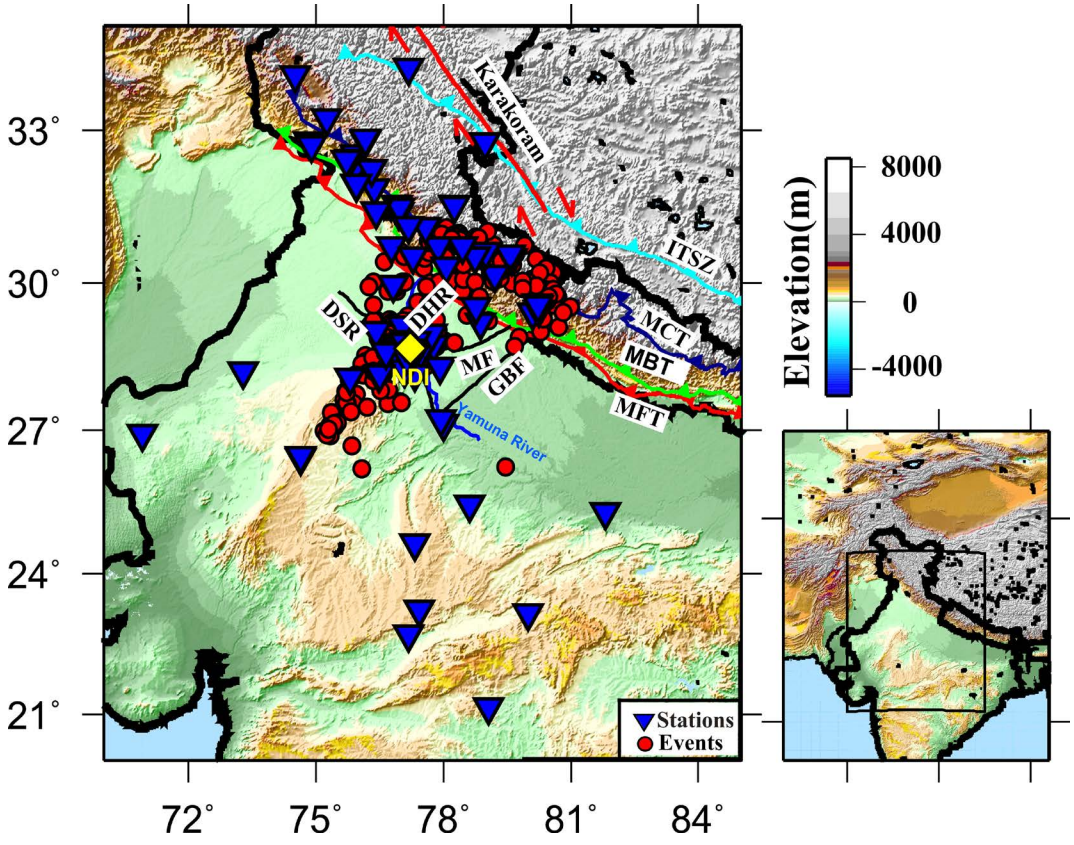

Figure 1. The seismicity map of Central Northern India showcases significant regional tectonic attributes linked with the Himalayan region, encompassing geological features such as the Main Frontal Thrust (MFT), Main Boundary Thrust (MBT), Main Central Thrust (MCT), Indus-Tsangpo Suture Zone (ITSZ), Karakoram Fault (KF), Delhi-Hardwar Ridge (DHR), Moradabad Fault (MF), Mathura Fault (MTF), and Great Boundary Fault (GBF). The distribution of seismic events is represented by red circles, occurring at various focal depths. Additionally, Seismic observatories of the NCS are represented by black triangles, while a yellow diamond indicates the NDI station as a reference point. The topography data of the global relief model (ETOPO.1) can be accessed through the provided (https://www.ngdc.noaa.gov/mgg/global/relief/ETOPO1/data/bedrock/grid_registered/netcdf/) link.

Moradabad Fault (MF), the Great Boundary Fault (GBF), the Delhi-Hardwar Ridge (DHR), the Mathura Fault (MTF), the Delhi-Lahore Ridge (DLR), and the Sohna Fault (SF). In addition to these prominent geological features, the region also encompasses a variety of less conspicuous linear formations and distinct tectonic characteristics. This intricate network of faults and tectonic elements, along with several minor linear features and more distant geological structures, contribute to the region's seismic profile. These elements are depicted in Figure 1, providing a visual representation of the complex tectonic landscape surrounding Central Northern India.

The investigation of earthquake-induced ground motion characteristics in the Delhi region and its surroundings has led to significant advancements in our understanding of the area's seismicity. Noteworthy contributions in this regard include the studies by Bansal et al. [2022] and Mittal et al. [2015, 2023], which have provided a deeper insight into the seismic behavior of this region.

The Moho thickness beneath the Delhi Fold Belt (DFB) is reported to be between 40 to 44 km, with an average depth of approximately 43 km, according to analyses by Mitra et al. [2011] and Borah et al. [2015] using receiver function analysis. Meanwhile, the crustal thickness in the Aravalli-Delhi Fold Belt (ADFB) varies more widely, ranging from 38 to 50 km as determined by Mandal et al. [2013] through common reflection stacking (CRS). These findings highlight the variation in the crust-mantle boundary within these regions.

Despite these valuable findings, it's important to acknowledge that the current models for this region still suffer from limited resolution in the crust, a challenge that has persisted even with numerous research efforts. To address this limitation, the present study has employed the VELEST program, originally developed by Kissling in 1988 and further refined by Kisling et al. in [1994]. This approach has enabled us to develop a more detailed velocity model that encompasses both P and S waves, providing a more reliable velocity model for the study region.

In the realm of seismology, extensive investigations have frequently relied on initial velocity models as fundamental reference points. However, the influence of these starting models on the outcomes of tomographic inversions has not been thoroughly scrutinized in prior research, as indicated by studies like Singh [1999] and Medved et al. [2022]. It's imperative to recognize that an inadequately calibrated initial reference model can greatly diminish the quality of the final solution, introducing significant uncertainties in the results. To address this issue, the present study has embarked on a meticulous evaluation of the 1-D velocity model specifically for central northern India, focusing on Delhi and its surrounding areas. This evaluation was conducted using a joint inversion methodology that integrates travel time residuals, station corrections, and refined hypocenter coordinates. The culmination of this process has resulted in a minimum 1-D velocity model that stands as a robust and localized model for our study region. This model significantly enhances the precision and reliability of our determinations of source parameters. Further, the importance of the present study cannot be overstated, especially considering the critical role of earthquake parameters in accurately evaluating the seismic hazard of the National Capital Region (NCR) Delhi, as this area is not only densely populated and industrially significant but also witnessing a rapid proliferation of high-rise buildings.

2. Data and Methodology

For the evaluation of hypocentral parameters, including P and S wave arrivals, we gathered data from the seismological bulletins of the International Seismological Centre (ISC) [available at http://www.isc.ac.uk/cgi-bin/collect?Reporter=NDI] and the National Center for Seismology (NCS) [accessible via https://seismo.gov.in/bulletins]. Our dataset spans 20 years, from January 2000 to July 2020. In this study, eighty-four seismological stations, located in northern central India including NCR-Delhi, played a critical role in determining the 1-D crustal velocity structure of the area. The seismological observatories are equipped with both broadband seismometers like Nanometrics Trillium-240 and Reftek 150B-120, as well as accelerometers (Metrozet TSA-100S, and Reftek 147A) featuring a 6-channel, 24-bit data logger and GPS time receiver, with VSAT terminal for real-time transfer of ground motion data to the 24x7 Operational Centre at New Delhi. The details related to the date of installation and up gradation for each observatory are given at www.seismo.gov.in and discussed in detail by Bansal et al. [2021], Dattatrayam et al. [2014], and Bhattacharya and Dattatrayam [2000]. All these seismic network setup has been instrumental in acquiring the necessary data for the present study.

For the processing of the acquired data towards determining the 1-D velocity model, the VELEST program [Kissling, 1988; Kissling et al., 1994], and to derive the local magnitude scale MAG2 program within the SEISAN software [Havskov and Ottemoller, 1999] were employed.

The HYPOCENTER program [Lienert et al., 1986] was used to ascertain the precise location of seismic events and to calculate the local magnitude. For the calculation of theoretical travel times, the AK135 velocity model [Kennett et al., 1995] for continental structure was initially used. Initially, P and S wave arrival times with travel time residuals exceeding 2.0 seconds and 3.0 seconds, respectively, were excluded. The events were then relocated using the refined P- and S-arrival data. To ensure the accuracy of earthquake locations, a stringent selection process was applied. This process led to the inclusion of 413 earthquakes that met the following criteria: (a) data availability from at least eight stations, (b) an azimuthal gap smaller than 180 degrees, and (c) root mean square (RMS) residuals of travel time within 2.0 seconds. The final dataset included a total of 3,191 P-arrivals and 2,986 S-arrivals, which

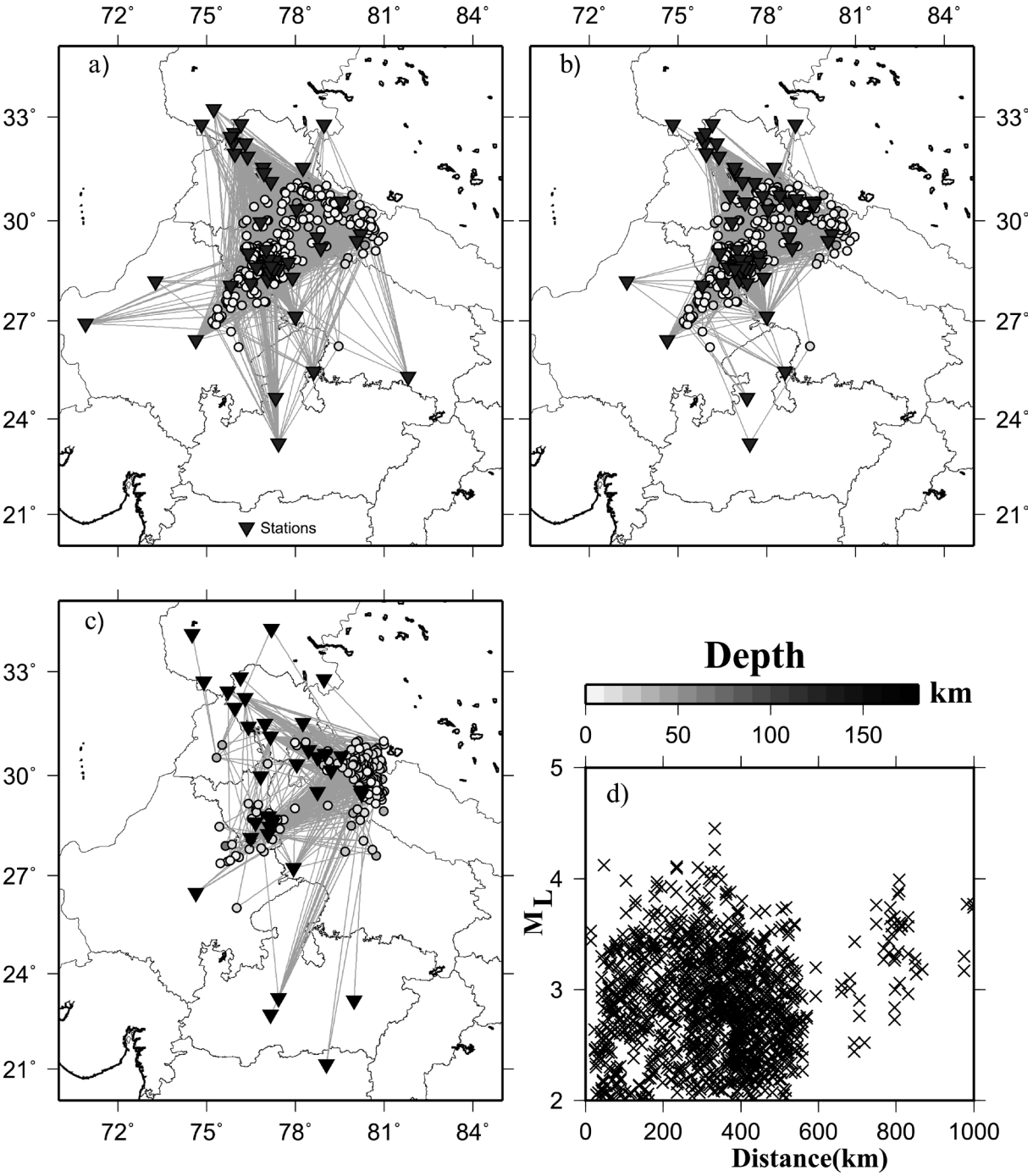

Figure 2. (a) 1D seismic velocity inversion uses the P-wave coverage of the earthquake ray path (shown by circles). (b) S-wave ray-path coverage. (c) M_L scale inversion (MAG2 program) uses 166 earthquakes ray-path coverage. (d) Data distribution of M_L scale with distance as per Hutton and Boore [1987].

were recorded across various seismological stations. The ray paths of these arrivals effectively covered the entire study region, as depicted in Figures 2a and 2b.

A key aspect of analysis in this study includes determining the local magnitude scale. The process involves measuring the maximum amplitude of the horizontal components (from zero to peak in nanometers) corresponding to S or Lg waves. These measurements were taken from Wood-Anderson (WA) seismograms generated using instrument response. The raw digital seismogram was corrected to account for the specific recording instrument, producing a displacement trace. This trace was then multiplied by the response function of a WA instrument to simulate how the seismic event would have appeared on an original WA seismograph. The maximum amplitude measured on these S-wave displacement seismograms was then used to determine the local magnitude of the event, which in turn contributed to establishing the local magnitude scale for the study region.

2.1 1-D Velocity Model

Seismic tomography is fundamentally a nonlinear process. Typically, solutions are obtained through linearization with respect to an initial reference model. The resulting tomographic images generated through this linearized inversion process are influenced by both the initial reference models and hypocenters [Kissling et al., 1994]. To tackle this issue, the VELEST program within the SEISAN software was used for a simultaneous inversion that includes the initial reference 1-D velocity model, hypocenter location, and station corrections, following methodologies established by Ellsworth [1978] and Kissling et al. [1994]. The accuracy of earthquake locations plays a crucial role in resolving the intricate details of the 1-D velocity model. Hence, this interconnected relationship between the 1-D velocity model and hypocenter locations is known as the linked hypocenter-velocity problem [Kissling et al., 1994]. To address this challenge, an inverse approach was employed, involving the linearization of the problem and using least square principles for deriving the solution. The key inputs for this methodological process included selecting an appropriate initial velocity model and compiling a high-quality dataset of P- and S-arrival times. This approach is critical in ensuring a comprehensive and accurate resolution of crucial attributes, particularly the number of layers and their respective thicknesses in the studied region.

2.2 Initial Reference 1-D Velocity Models

We commence our analysis considering the Indo-Gangetic (IG11) local seismic velocity model proposed by Bhattacharya [1992]. This model, structured into multiple layers, averages seismic velocities for both P-waves and S-waves within each layer, thus offering a detailed characterization of the seismic velocity structure at various depths in the study region. Similarly, the AK135 velocity model [Kennett et al.,1995] was also employed, which is similarly divided into layers with averaged velocities of P and S waves. Julia et al. [2009] studied the seismic velocity model beneath the Indian shield through a joint inversion of receiver functions and surface wave group velocities. The study proposed the seismic velocity model at the NDI station, which was used in the present study as one of the initial models for the VELEST inversion procedure.

Borah et al. [2015] investigated the seismic velocity structure beneath the Indo-Gangetic Plain and its adjacent Himalayan region, using receiver function analysis. Similarly, Rai et al., [2006] probed the seismic velocity structure beneath the Northwest Himalayas and Ladakh, employing receiver function analysis. These five models are illustrated in Figure 4 and detailed in Table 1. They are also employed in the inversion process of the VELEST program as an initial reference model to test the lowest travel-time rms residuals for each model.

2.3 Inversion for Velocity Model

The crust was initially divided into five-kilometer layers, with the addition of two 5-kilometer-thick layers below the expected Moho depth to test the Moho depth. This approach, as recommended by Kissling et al. [1995], was adopted to evaluate the Moho depth since layer thicknesses are not subject to inversion.

The velocities for these layers were interpolated from the original models, taking into account the gradual increase in velocities with depth.

This systematic approach in the inversion process aimed to converge toward the most favorable solution, offering an enhanced depiction of the crustal velocity structure (Figure 3). The procedure involved a two-step approach. The first step involved determining the hypocentral location using the HYPOCENTER program. Subsequently, in the second step, velocity model inversion was concurrently performed with hypocenter relocations. This process was iterated up to 10 times, and layers that exhibited identical velocities were merged into a single layer.

To determine the most effective model among the initial set, each model was subjected to an additional random initial model test. This involved 500 perturbations for each model, where random V_P and V_S values were generated

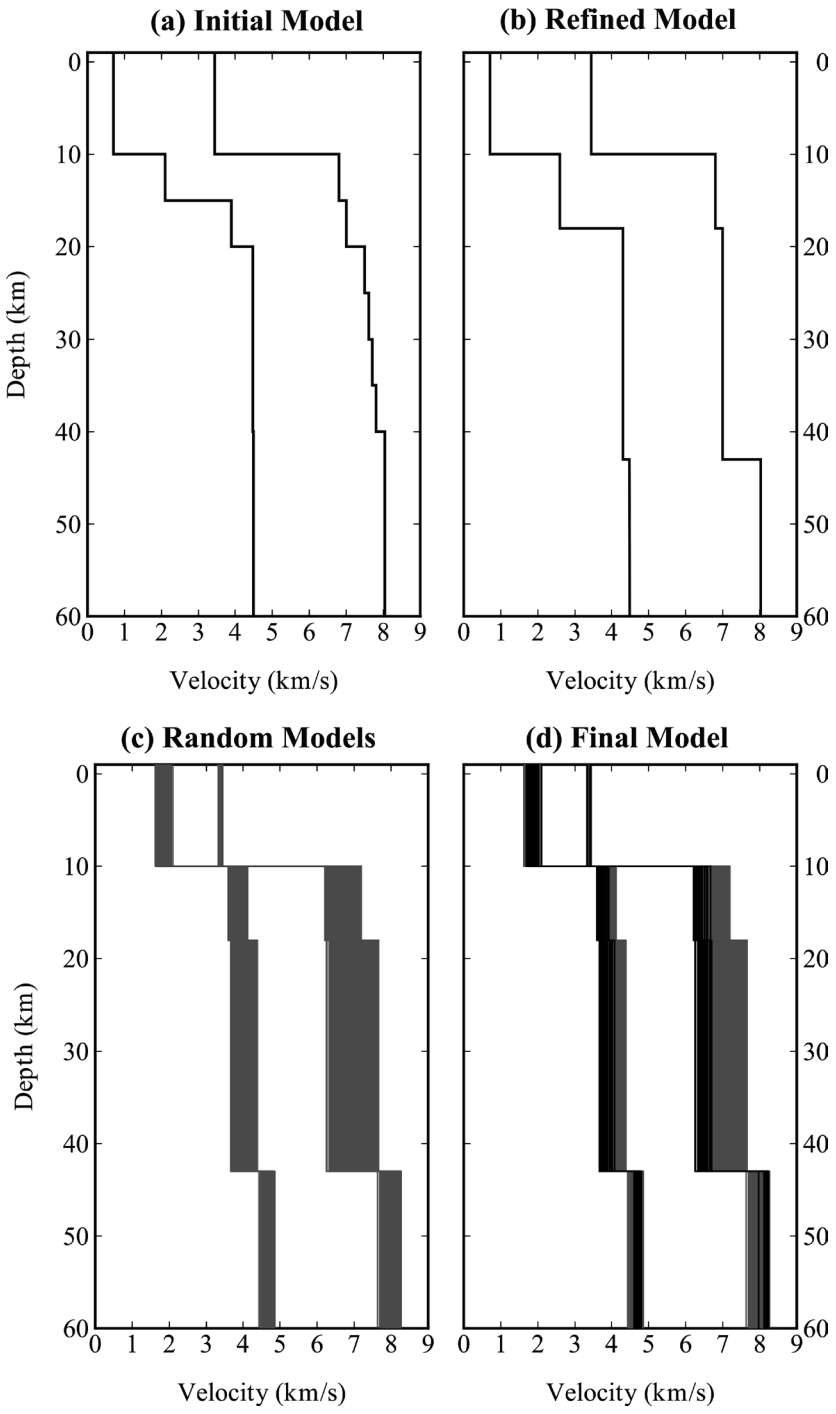

Figure 3. Steps for the IG11 model's inversion procedure. (a) Initial model with a mantle thickness of 10 km and a crustal layer thickness of 5 km. (b) The refined initial model was obtained through inversion and merging of layers with alike velocities. (c) Starting models for the initial random test. (d) Results of the arbitrary preliminary test, with approved models shown in black and all inverted models shown in dark grey.

within a ±10% range for each layer. During these perturbations, the V_P/V_S ratio was kept constant, falling within the limits of 1.6 to 1.9. The VELEST program was used to conduct the inversion procedure for each perturbed model.

Following the recommendations of Kissling et al. [1994], specific damping settings were applied, including damping at the origin time set to 0.01, hypocentral damping at 0.01, depth damping at 0.01, velocity damping at 1.0, and station damping at 1.0. Additionally, the maximum iteration limit for each model was set to 10. This methodical approach aimed to ensure the stability and accuracy of the inversion process, enabling the identification of the most reliable seismic velocity model.

We conducted a preliminary model test to determine the optimal velocity model. This involved generating 500 perturbations for each model by randomly adjusting the values of both P-wave velocity (V_P) and S-wave velocity (V_S) within a range of ±10% for every layer. We ensured that the V_P to V_S ratio remained within the range of 1.6-1.9 throughout the modifications. Subsequently, we apply station correction fine-tuning using the final velocity model with a higher damping value of 10.0, following the method outlined by Husen et al. [2011]. Although the velocity model remains largely unaltered, the inversion process updates the station correction and hypocenters. For this purpose, the NDI station, located in the central part of the study region on exposed hard rock and continuously operational throughout the data collection period, was designated as the reference station.

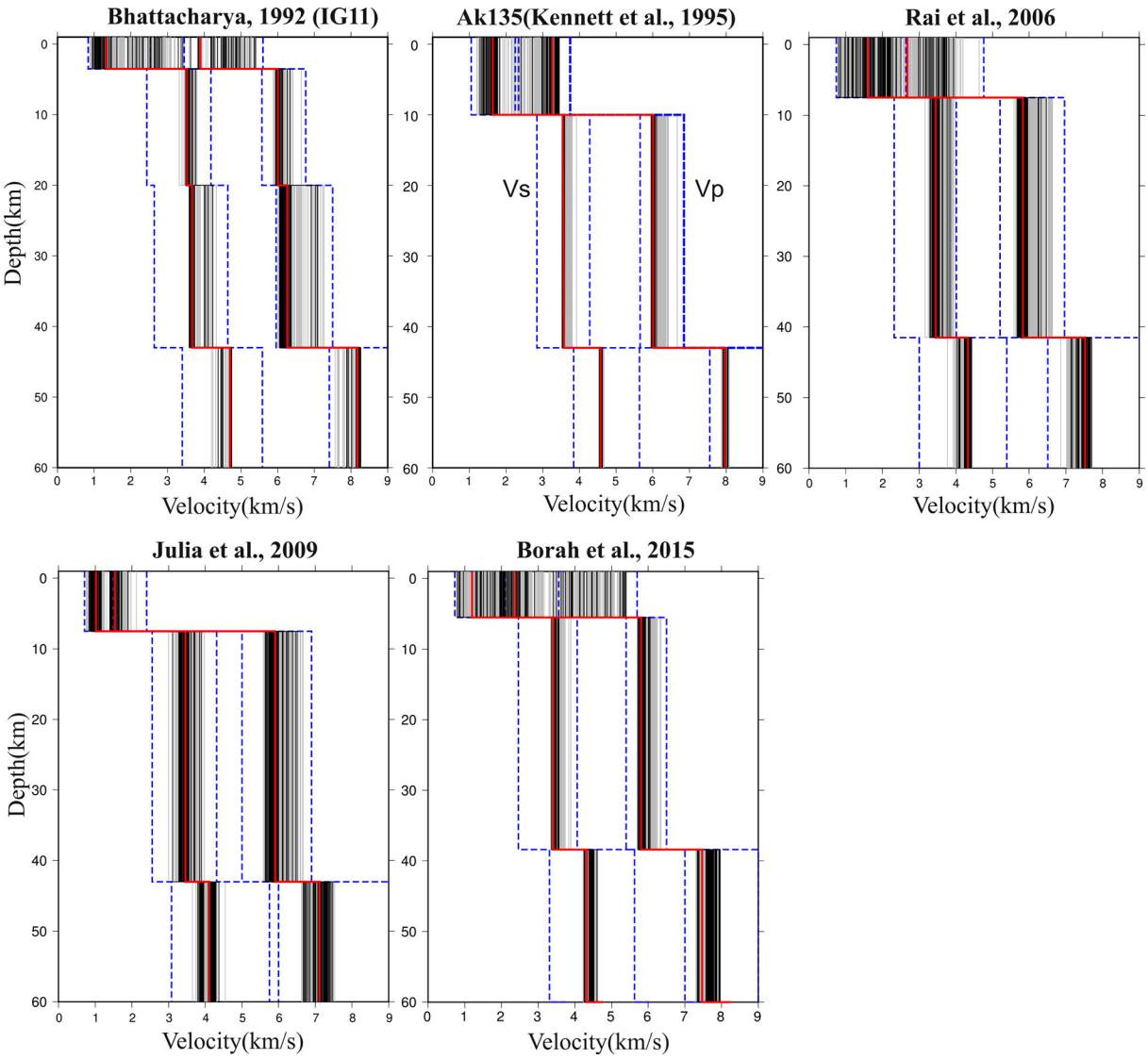

Figure 4. The accepted velocity models are represented by the black lines, which are identified as the best solutions. The gray lines depict all of the approved outcomes obtained in 500 iterations. The red solid line corresponds to the final accepted model, which stands as the most precise and reliable representation of the seismic velocity structure.

To rigorously evaluate the quality of the inversion solution derived from the VELEST program, the HYPOCENTER program within SEISAN was used to re-locate the seismic events. This process involved applying the ultimately approved velocity model along with station corrections. The new 1-D velocity model IG11 by Bhhatacharya, 1992 showed the lowest RMS residuals based on average weighted RMS travel-time residuals. A comparison of the initial and final model for the travel-time RMS values is presented in Table 1. The utilization of this refined final velocity model is expected to significantly enhance the precision in determining earthquake locations, offering a more accurate and reliable understanding of seismic activity in the study area.

3. Local Magnitude Inversion

The National Center for Seismology presently uses the local magnitude scale (M_L) developed by Hutton and Boore [1987] for southern California. However, the distinct tectonic features of central northern India, particularly the alluvium soil of the Indo-Gangetic plains, necessitate a reassessment of this scale's appropriateness for the region. This evaluation is crucial to establish whether a more accurate, region-specific magnitude scale, better suited to the unique geological characteristics of the area, can be developed. Therefore, identifying an appropriate local magnitude scale for the study region to enhance the accuracy of magnitude estimations.

Richter [1935] initially proposed the local magnitude scale (M_L) as a means to assess the magnitude of earthquakes. This scale relies on the measurement of the maximum amplitude derived from the horizontal-component seismogram recorded using the WA seismograph. While the seismogram was previously analog, the digital raw waveform has now been transformed into an equivalent WA seismogram that has a period of 0.8 seconds, and a factor of damping 0.8 [Ottemöller and Sargeant, 2013]. Richter [1935] first introduced the M_L as

$$M_L = \log \mathrm{A} - \log \mathrm{A0} + \mathrm{S}, \tag{1}$$

Here amplitude is A and measured in millimeters with a gain of 2080 by the WA seismograph.
S is the station correction, while –log A0 is the epicentral-distance-dependent correction factor.

Later on, Bakun and Joyner [1984] extended the use of the M_L scale to central California and introduced the correction term as.

$$-\log \mathrm{A0} = \mathrm{a} \log\left(\frac{R}{100}\right) + \mathrm{b}(\mathrm{R} - 100\ \mathrm{km}) + 3.0, \tag{2}$$

The coefficients "a" and "b" in this case are dependent on the geometric attenuation and spreading, respectively. The hypocentral distance "R" is measured in kilometers. Hutton and Boore [1987] derived the values of the constants, with "a" equal to 1.11 and "b" equal to 0.00189, specifically for the southern California region.

The present analysis focused mainly on earthquakes with depths shallower than 50 km. The dataset comprised a total of 166 earthquakes and each event comprises at least 3 amplitudes. Among these, we considered 1404 maximum amplitudes of S- and Lg waves.

The coverage of ray paths for the selected event (166 earthquakes) used for M_L inversion, and the distributed data w.r.t. the M_L scale for southern California [Hutton and Boore, 1987] are shown in Figure 2c and 2d respectively.

The primary objective is to estimate a unified magnitude scale that encompasses the entire central north India comprising mainly Delhi and its surroundings. To achieve this, an analysis of data distribution with distance was conducted and compared to the previously established scale i.e., the southern California M_L scale, as depicted in Figure 5. The dataset consists of signal amplitudes recorded from hypocentral distances up to 1000 km, predominantly featuring events within an epicentral distance of 400 km. The magnitudes observed in this study range from M_L 2.0 to 5.2. Given the geological characteristics of the area, necessitating the application of correction terms to the M_L scale due to different seismic wave attenuation. The following equation is used to address these variations:

$$M_L = \log \mathrm{A}\,(\mathrm{nm}) + \mathrm{a} \log(\mathrm{R})\,(\mathrm{km}) + \mathrm{bR} + \mathrm{C} + \mathrm{S} \tag{3}$$

To estimate parameters such as M_L, a, b, the base level C, and S, an inversion process using the singular value decomposition method was carried out. Ottemöller and Sargeant [2013] described this method, which was implemented through the MAG2 program within the SEISAN software package [Havskov and Ottemoller, 1999].

To assess the effectiveness of this method, a comparative analysis was performed on the residuals of M_L calculated using the Southern California scale [Hutton and Boore, 1987] without station correction and, this study with station corrections. This analysis also included a comparison with the new M_L values calculated for the current study region, which incorporate station corrections, as illustrated in Figure 5. The results indicated that the new scale, when adjusted with station corrections, exhibited significantly lower residuals compared to the Southern California scale without station corrections. Finally, the study derived the following M_L scale from the equivalent WA digital seismogram with unity gain, tailored to the unique seismic environment of central northern India:

$$M_L = \log \mathrm{A\,(nm)} + 0.752 \times \log \mathrm{R\,(km)} + 0.00129 \times \mathrm{R\,(km)} - 1.315 + \mathrm{S} \tag{4}$$

This new scale highlights the importance of customizing the magnitude scale to the specific seismic characteristics of the study region.

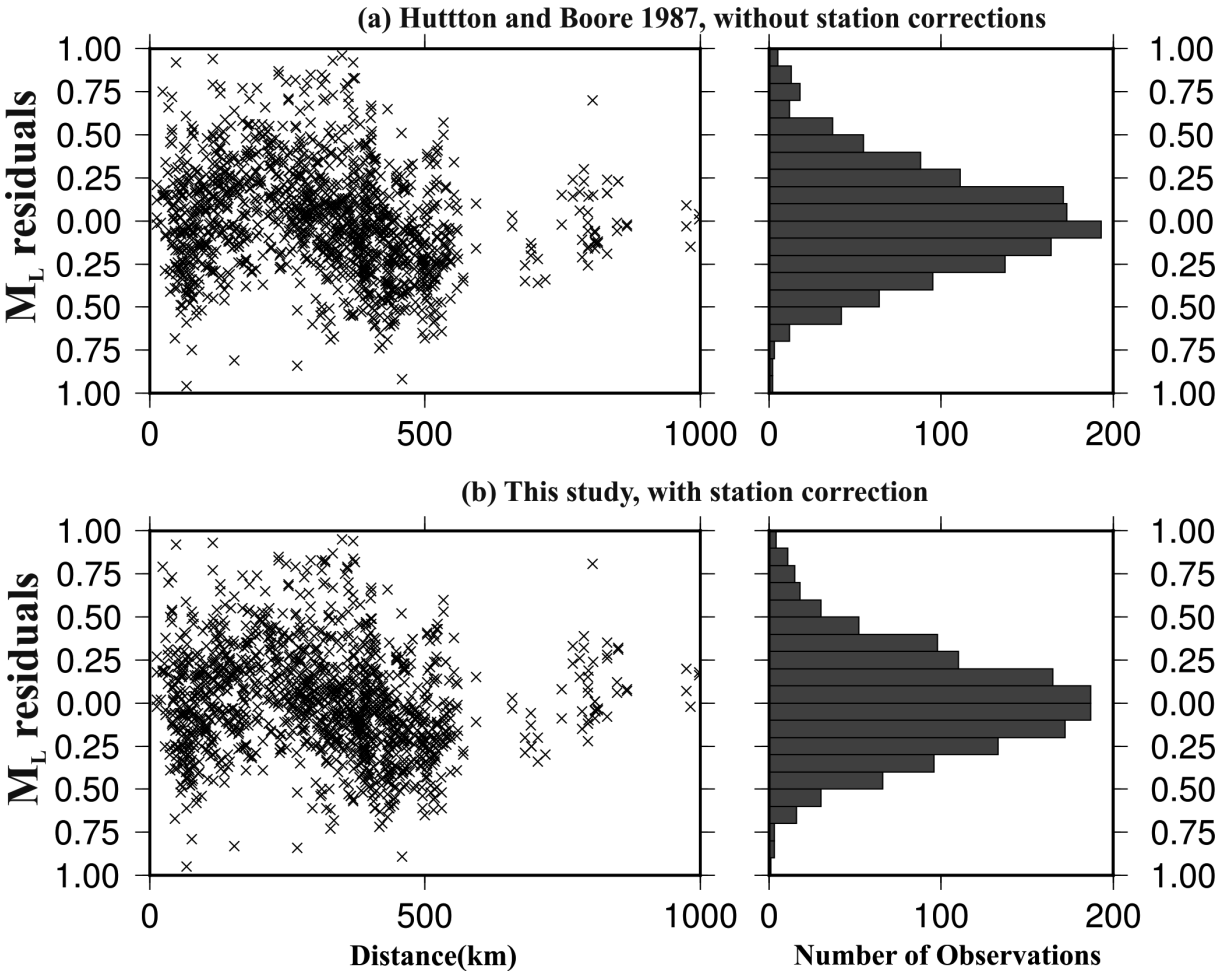

Figure 5. The left panel displays M_L residuals versus distance, and the right panel displays M_L residuals versus the number of observations (a) Without station correction according to the M_L scale from Hutton and Boore in 1987. (b) The present study with station corrections.

4. Result and Discussion

The current study involved an extensive analysis of the National Center for Seismology (NCS) Seismological bulletins and the ISC (International Seismological Centre) catalog, spanning from January 2000 to July 2020. This research specifically focused on seismic stations operated by the NCS, which play a crucial role in real-time earthquake monitoring. To enhance the study's reliability, amplitudes corresponding to hypocentral distances under 1000 km were meticulously selected, with the majority falling within the range of 400 km.

The approach to seismic velocity inversion focused on events at focal depths less than 50 km. This study analyzed a dataset comprising 413 earthquakes, which were recorded by 85 stations. Five distinct models were employed to conduct the analysis, with a comparison of the root mean square (RMS) values, as detailed in Table 1.

The lowest RMS travel time was achieved using the final model from Bhattacharya [1992] (IG11). Consequently, this IG11 model has been identified as the most appropriate option, as detailed in Table 2. and hence considered as the best initial model for the inversion (Figure 6).

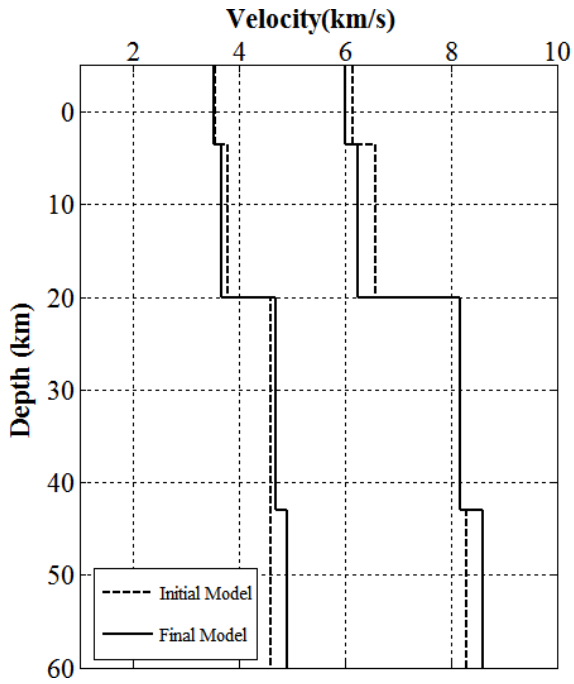

Figure 6. Comparison between initial and final velocity models of the Bhattacharya [1992] IG11 model, highlighting the one with the minimum root mean square (RMS) value.

The comparison of initial and final mean residual travel times is shown in Table 1. The model IG11 exhibited the minimum residual travel time of 1.281 and was thus considered the best initial model. The obtained new model is named "CNI24," representing "Central Northern India (CNI)" and denotes the year 2024.

The current investigation unveils P-wave and S-wave velocities at the Moho of 8.18 km/s and 4.71 km/s, respectively. These values are slightly higher than those observed in all other models used for comparison (Figure 7 and Table 2). These variations indicate that the crustal velocity in the Indian shield, especially in central northern India, is higher than in the Himalayan region, as supported by Singh et al. [2017]. The slightly higher velocities suggest a denser geological structure in the study area, indicating a more compact crust, similar to that of the peninsular shield.

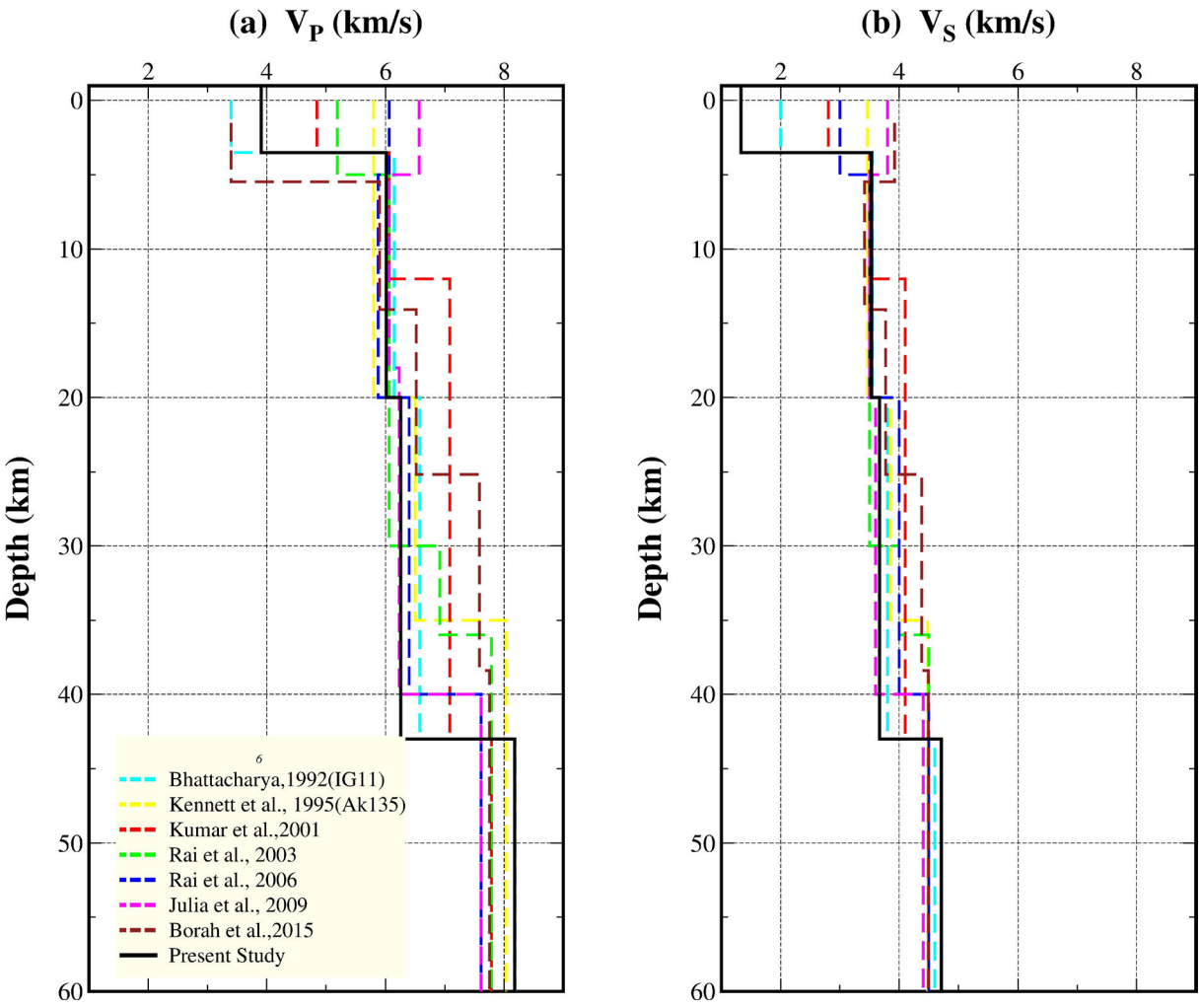

Figure 7. The present study compares the seismic velocities of the present study with local and regional models (a) P wave plot and (b) S wave plot.

Sr. no.	Velocity Model	Initial Mean Residual [sec]	Final Mean Residual [sec]
1	AK135 [Kennett et al., 1995]	1.819	1.325
2	Bhattacharya, 1992	1.338	1.281
3	Julia et al., 2009	1.661	1.649
4	Rai et. al., 2006	1.627	1.545
5	Borah et al., 2015	1.501	1.474

Table 1. Comparison of Initial and Final Models Mean Residual Time.

Initial Model (IG11)			Final Model (CNI24)	
Depth [km]	Vp [km/s]	Vs [km/s]	Vp [km/s]	Vs [km/s]
0	3.40	2.00	3.90	1.33
3.5	6.15	3.55	6.01	3.53
20.0	6.58	3.80	6.26	3.67
43.0	8.19	4.60	8.18	4.71
100.0	8.30	4.60	8.60	4.91

Table 2. Comparative Analysis of Seismic Velocities at Varied Depths between Initial (IG11) and Final (CNI24) Models.

The travel time residual error improved significantly, dropping from 1.338 in the initial velocity model IG11 to 1.281 in the final CNI24 model. The new CNI24 model features a 3.5 km thick sediment layer with a P-wave velocity of 3.90 km/s, which is underlain by lower crustal layers extending down to 20 km and then to 43 km, with P-wave velocities of 6.01 km/s and 6.26 km/s, respectively (Table 2). The Moho boundary is at a depth of 43 km, where the P-wave velocity is 8.18 km/s and the S-wave velocity is 4.71 km/s.

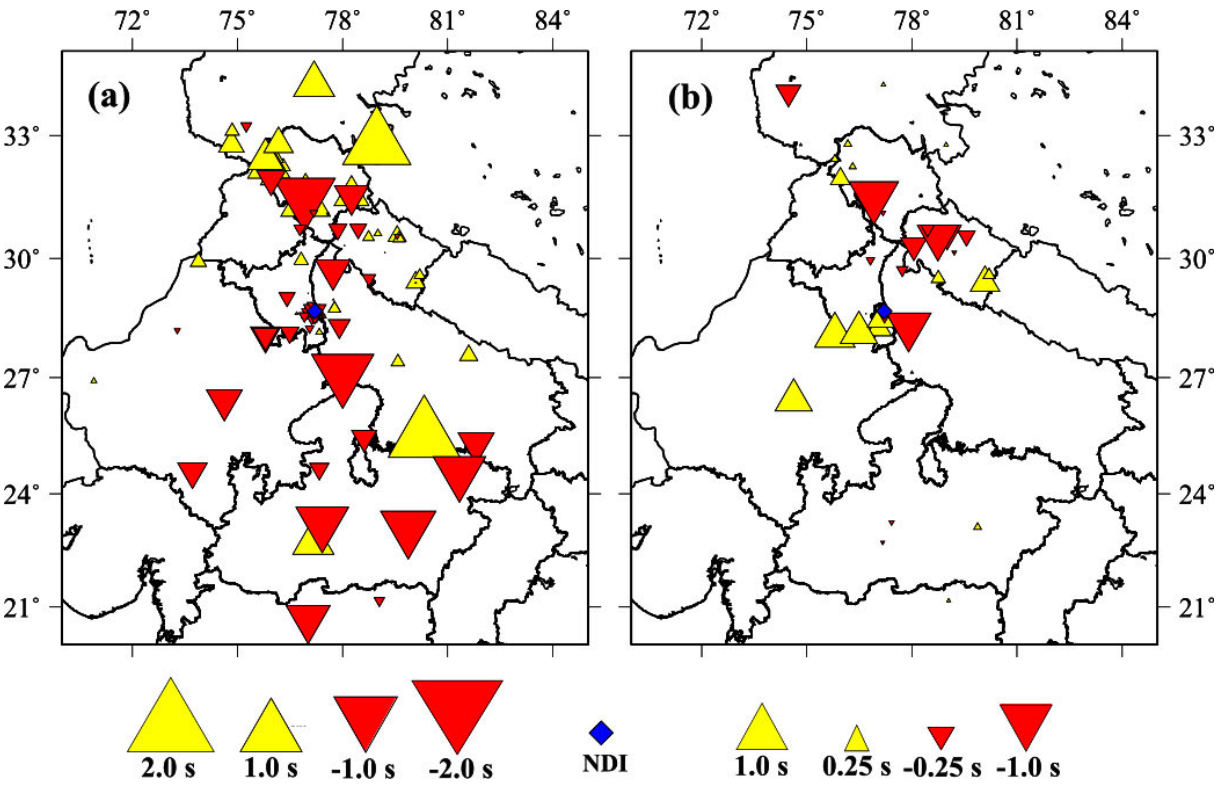

Figure 8. (a) Displays the P-wave station corrections (Table S1, Supplementary material) derived from the VELEST, corresponding to the IG11 model. The blue diamond represents the reference New Delhi (NDI) station. (b) Shows the magnitude station corrections (Table S2, Supplementary material) for the M_L scale.

The new dataset, comprising 46 events from August 2020 to February 2023, was analyzed but not included in the inversion process of the VELEST program. Using both the IG11 and new CNI24 velocity models (Table 2 for the CNI24 final model), the hypocenters were re-located using the HYPOCENTER program in the SEISAN software. This was done separately for both IG11 and the newly developed CNI24 model. The analysis revealed that the CNI24 model reduces the average root mean square (RMS) error of travel time residuals by 0.04 seconds. It also decreases horizontal (ERH) and vertical (ERZ) errors by 0.31 km and 0.40 km, respectively, compared to the previous IG11 model (Table S3 in the supplementary material).

The variation in crustal thickness and velocity can lead to prominent delays in arrival times. P- arrivals at stations located in the northern part of our research area are characterized by a noticeable time delay, indicated by positive delays (Figure 8, yellow color triangles). The potential causes for this time delay include the occurrence of reduced crustal velocity around the Himalayas. Conversely, the southern stations in the region display early P and S arrivals, represented by negative delays (triangles in red, Figure 8a), which could be associated with higher crustal velocity.

Several studies have highlighted the variability in Moho depths across India, particularly in the Delhi region with depths ranging from 36 to 46 km. Rai et al. [2006] noted a deepening of the Moho from about 40 km beneath Delhi to roughly 75 km beneath Taksha at the Karakoram Fault in the NW Himalaya region. In the southern shield, Rai et al. [2003] reported a similar Moho depth of around 36 km, while Kumar et al. [2001] observed a range of 33 to 39 km in the Indian shield. Julià et al. [2009] found a crustal thickness of 40 km beneath Delhi. Borah et al. [2015] observed fluctuations in crustal thickness in the Lesser Himalaya was found to have a constant thickness of 44 km. The Moho depth of 43 km in the present study aligns with these earlier findings. Moreover, the present study's P and S wave velocities at the Moho, at 8.18 km/s and 4.71 km/s respectively, are slightly higher than those reported in previous models.

4.1 Local Magnitude Scale (M_L)

The comprehensive analysis detailed earlier led to the derivation of a local magnitude scale (M_L) specifically designed for the study region:

$$M_L = \log \mathrm{A\,(nm)} + 0.752 \times \log \mathrm{R\,(km)} + 0.00129 \times \mathrm{R\,(km)} - 1.315 + \mathrm{S} \tag{5}$$

The scale is applicable for magnitudes up to 4.6 and hypocentral distances of 1000 km.

Additionally, another inversion was carried out where the values of a and b were held constant according to the Southern California scale [Hutton and Boore, 1987]. This involved comparing the residuals of the M_L scale with and without station corrections for the study region. Without station corrections the M_L scale for Southern California and the present study region both have smaller residuals than the scale for Southern California, which shows that local site variation has a substantial impact on maximum amplitudes.

The M_L distance correction term ($\mathrm{a} \times \log \mathrm{R} + \mathrm{b} \times \mathrm{R} + \mathrm{c}$) was compared with correction terms for other regions that is, southern California [Hutton and Boore, 1987], central California [Bakun and Joyner, 1984], eastern United States [Kim, 1998], and Norway [Alsaker et al., 1991] (Figure 9). It is found that the distances up to ~100 km, the present study's M_L distance correction term is larger than the southern California scale.

For distances spanning up to 400 km, where our observations are present, the correction is somewhat higher compared to the eastern United States [Kim, 1998] and Norway [Alsaker et al., 1991] scales. However, for distances greater than 500 km, the correction term gradually diminishes as the distance increases, though it remains lower than that of southern California [Hutton and Boore, 1987] and central California [Bakun and Joyner, 1984], as shown in Figure 9. These findings indicate that the geological differences play a significant role in influencing the maximum ground amplitude we observe and hence the correction term.

With station correction, the new M_L scale leads to a significant reduction in M_L residuals shown in Figure 8b. Further, both the scales (M_L) used for southern California and the scale applied in the present study region, after making station corrections, show smaller differences when compared to the southern California scale without station corrections. The variations in '*a*' and '*b*' values further indicate distinct crustal structures between central northern India and southern California. Complementing this, a comparative analysis of seismic moment magnitude (Mw)

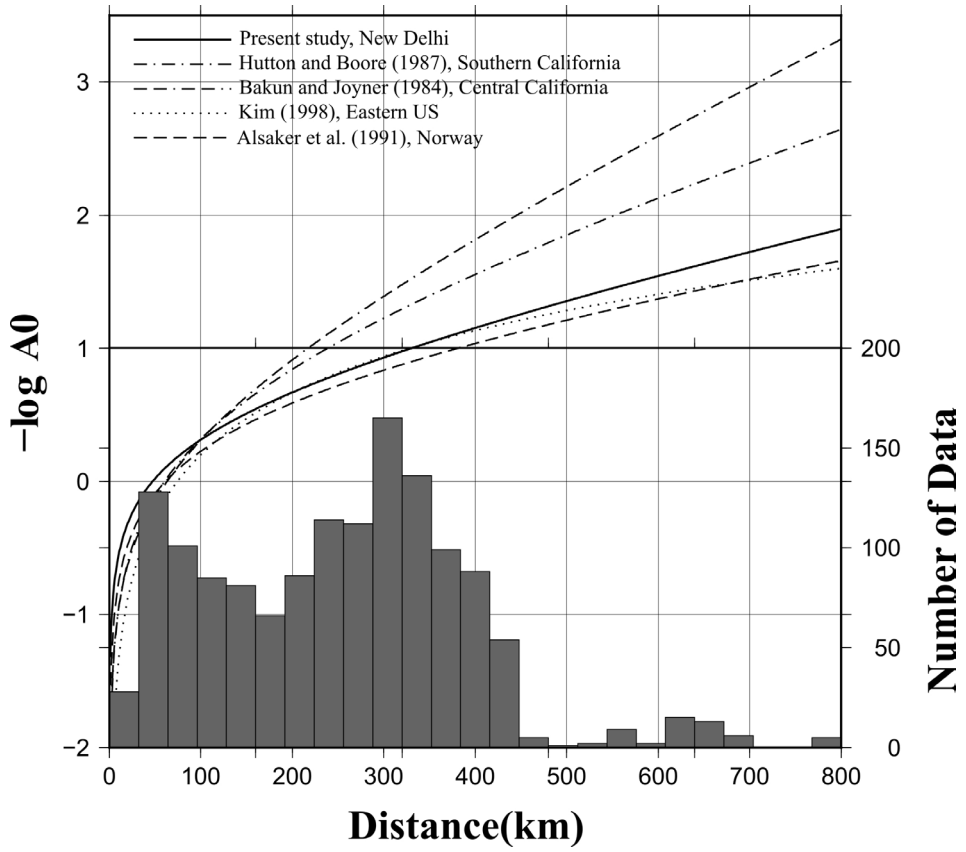

Figure 9. Comparison of the present study with other regions M_L correction terms for unit displacement in nanometers. Additionally, the histogram below the curve depicts the distribution of data used at various hypocentral distances.

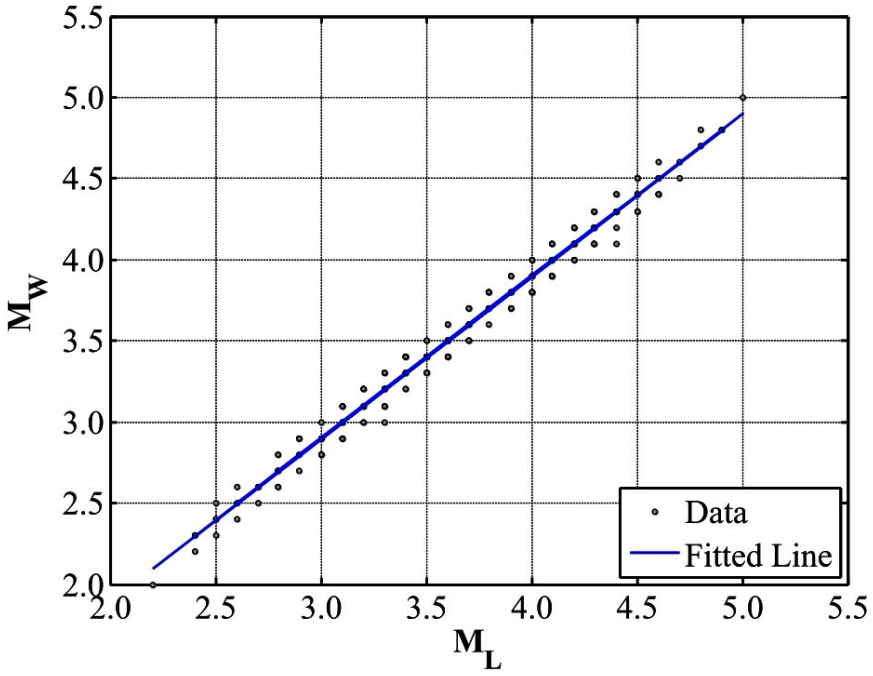

Figure 10. The error bars, representing a variability of ±0.10 around the regression line, highlight the inherent uncertainty in converting magnitudes. Notably, the Mw aligns closely with the newly established M_L scale. The close alignment of Mw with the new M_L scale reaffirms its suitability for the current study area, providing a more accurate representation of local seismic magnitudes in this region.

and the new local magnitude (M_L) for 254 seismic events using linear orthogonal regression. This relationship is expressed by the equation $\mathrm{Mw} = (1.0)M_L \pm 0.10$, demonstrating a linear correlation between the two magnitude scales (Figure 10).

5. Conclusion

The current study successfully demonstrated the efficacy of a newly developed local magnitude scale and a 1-D crustal velocity model tailored for the central northern Indian region. This advancement, which incorporates station corrections, has shown significant improvements in the accuracy of earthquake location and local magnitude estimation.

The new 1D model has proven its reliability in determining hypocenter solutions for shallow earthquakes by using various crustal phases (Pn, Pg, Sg, and Sn), simultaneously reducing uncertainties related to earthquake depths and performing better than any of the previously determined velocity models. So, the present study using the VELEST approach has resulted in a refined velocity model, surpassing earlier versions in accuracy.

Moreover, the introduction of the new M_L scale, when combined with station corrections, yielded lower residuals than those observed with the Southern California scale. This outcome underscores the effectiveness of the proposed approach, particularly considering the tectonic complexity and lateral variations in Delhi. These findings are instrumental in achieving more reliable earthquake locations and magnitude estimations, which are crucial for enhancing seismic studies and deepening our understanding of earthquakes in the region.

Information and Sources. The seismic data used in this research were collected from reliable sources, including the seismological bulletins of the International Seismological Centre (ISC) for the study region (http://www.isc.ac.uk/cgi-bin/collect?Reporter=NDI) (last accessed April 2024) and the website of National Center for Seismology (NCS) (https://www.seismo.gov.in/bulletins) (last accessed April 2024). This dataset encompasses a period of 20 years, spanning from January 2000 to July 2020, with the addition of a new dataset (for validity of results) covering the period from August 2020 to February 2023.

The figures presented in this study were generated using the Generic Mapping Tools (GMT) software (version 5.0, [https://www.generic-mapping-tools.org/], last accessed May 2024; Wessel et al., 2013). Figure 1 utilized topography data from the EOTOPO.1 Global Relief model, which was obtained from https://www.ngdc.noaa.gov/mgg/global/ (last accessed May 2024).

References

Alsaker, A., L.B. Kvamme, R.A. Hansen, A. Dahle and H. Bungum (1991). The ML scale in Norway, Bull. Seismol. Soc. Am., 81 (2): 379-398. doi: https://doi.org/10.1785/BSSA0810020379

Bakun, W.H. and W.B. Joyner (1984). The ML scale in central California, Bull. Seismol. Soc. Am., 74(5):1827-1843. doi: 10.1785/BSSA0740051827

Bansal, B.K., A.P. Pandey, A.P. Singh, G. Suresh, R.K. Singh and J.L. Gautam (2021). National seismological network in India for real-time earthquake monitoring, Seismol. Res. Lett., 92, 4, 2255-2269. https://doi.org/10.1785/0220200327

Bansal, B.K., S.K. Singh, G. Suresh and H. Mittal (2022). A source and ground motion study of earthquakes in and near Delhi (the National Capital Region), India, Nat. Hazards, 111, 2, 1885-1905, https://doi.org/10.1007/s11069-021-05121-w

Bhattacharya, S.N. and R.S. Dattatrayam (2000). Recent advances in seismic instrumentation and data interpretation in India, Current Sci., 791347-1358.

Bhattacharya, S.N. (1992). Crustal and upper mantle velocity structure of India from surface wave dispersion, Current Sci., 62, 1/2, 94-100, http://www.jstor.org/stable/24095321

Borah, K., N. Kanna, S.S. Rai and K.S. Prakasam, (2015). Sediment thickness beneath the Indo-Gangetic Plain and Siwalik Himalaya inferred from receiver function modelling, J. Asian Earth Sci., 99, 41-56, https://doi.org/10.1016/j.jseaes.2014.12.010

Bureau of Indian Standards (BIS) (2016). IS 1893 (part 1): 2016 (Draft)—Indian standard criteria for earthquake resistant design of structures, part 1: General provisions and buildings (Sixth Revision), Bureau of Indian Standards, New Delhi, India

Chandra, U. (1992). Seismotectonics of the Himalayas, Current Sci., 62, 40-71.

Dattatrayam, R.S., G. Suresh, P.R. Baidya, R. Prakash, J.L. Gautam, H.P. Shukla and D. Singh (2014). Standards and methodologies of seismological data generation, processing and archival & guidelines for data sharing and supply, Proceedings of the Indian National Science Academy, 80, 3, 679-696. https://doi.org/10.16943/ptinsa/2014/v80i3/55143

Ellsworth, W.L. (1978). Three-dimensional structure of the crust and mantle beneath the island of Hawaii, Ph.D. Thesis, Massachusetts Institute of Technology, available at http: //hdl.handle.net/1721.1/52834 (Last accessed February 2024).

Havskov, J. and L. Ottemoller (1999). SeisAn Earthquake Analysis Software, Seismol. Res. Lett., 70, 5, 532-534.

Husen, S., E. Kissling and J.F. Clinton (2011). Local and regional minimum 1D models for earthquake location and data quality assessment in complex tectonic regions, Application to Switzerland, Swiss J.Geosci., 10, 3, 455-469, doi: 10.1007/s00015-011-0071-3.

Hutton, L.K. and D.M. Boore (1987). The Ml scale in Southern California, Bull. Seismol. Soc. Am., 77, 6, 2074-2094.

Julià, J., S. Jagadeesh, S.S. Rai and T.J. Owens (2009).Deep crustal structure of the Indian shield from joint inversion of P wave receiver functions and Rayleigh wave group velocities: Implications for Precambrian crustal evolution, J. Geophys. Res.: Solid Earth, 114, 10, 1-25, https://doi.org/10.1029/2008JB006261

Kennett, B.L.N., E.R. Engdah and R. Buland, (1995). Constraints on seismic velocities in the Earth from travel times, Geophys. J. Int., 122, 108-124, https://doi.org/10.1111/j.1365-246X.1995.tb03540.x

Kim, W.Y. (1998). The ML scale in eastern North America, Bull. Seismol. Soc. Am. 88, 4, 935-951.

Kissling, E. (1988). Geotomography with local earthquake data, Rev. Geophys., 26, 659-698. https://doi.org/10.1029/RG026i004p00659

Kissling, E., U. Kradolfer and H. Maurer (1995). VELEST User's Guide-Short Introduction, (Institute of Geophysics and Swiss Seismological Service, ETH Zurich), 25.

Kissling, E., W.L.L. Ellsworth, D. Eberhart-Phillips and U. Kradolfer (1994). Initial reference models in local earthquake tomography, J. Geophys. Res. 99, B10, 19,635-19,646.

Kumar, M.R., R. Kind, A.K. ShuklaSaul, D. Sarkar and J. Saul (2001). Crustal structure of the Indian Shield: New constraints from teleseismic receiver functions, Geophys. Res. Lett., 28, 7, 1339-1342, https://doi.org/10.1029/2000GL012310

Lienert, B.R., E. Berg and L.N. Frazer (1986). Hypocenter: An earthquake location method using centered, scaled, and adaptively damped least squares, Bull. Seismol. Soc. Am. 76, 3, 771-783.

Mandal, B., M.K. Sen, V.R. Vaidya and J. Mann (2013). Deep seismic image enhancement with the common reflection surface (CRS) stack method: Evidence from the Aravalli-Delhi fold belt of northwestern India, Geophys. J. Int., 196, 2, 902-917, https://doi.org/10.1093/gji/ggt402

Medved, I., I. Koulakov, S. Mukhopadhyay and A. Jakovlev (2022). Lithosphere structure in the collision zone of the NW Himalayas revealed by a local earthquake tomography, J. Geodyn., 152, May, 101922. https://doi.org/10.1016/j.jog.2022.101922.

Mitra, S., S.M. Kainkaryam, A. Padhi, S.S. Rai and S.N. Bhattacharya (2011) The Himalayan foreland basin crust and upper mantle, Phys. Earth Planet. Int., 184, 1-2, 34-40, https://doi.org/10.1016/j.pepi.2010.10.009

Mittal, H., A. Kumar, A. Kumar and R. Kumar (2015). Analysis of ground motion in Delhi from earthquakes recorded by strong motion network, Arabian J. Geosci., 8, 4, 2005-2017, https://doi.org/10.1007/s12517-014-1357-3

Mittal, H., B. Sharma, S. Arora and A. Ammani (2023). Characteristics of earthquake ground motions governing the damage potential for Delhi and the surrounding region of India, Quat. Sci. Adv., 12, July, 100098. https://doi.org/10.1016/j.qsa.2023.100098

Ottemöller, L. and S. Sargeant (2013). A local magnitude scale ML for the United Kingdom, Bull. Seismol. Soc. Am., 103, 5, 2884-2893, doi: 10.1785/0120130085.

Pandey, A.P., G. Suresh, A.P. Singh, A.K. Sutar and B.K. Bansal (2020). A widely felt Tremor (ML 3.5) of 12 April 2020 in and around NCT Delhi in the backdrop of prevailing COVID-19 pandemic lockdown: analysis and observations, Geoma., Nat. Hazazards Risk, 11, 1, 1638-1652, https://doi.org/10.1080/19475705.2020.1810785

Rai, S.S., K. Priestley, K. Suryaprakasam, D. Srinagesh,V.K. Gaur and Z. Du (2003).Crustal shear velocity structure of the south Indian shield, J. Geophys. Res.: Solid Earth, 108, B2, https://doi.org/10.1029/2002jb001776

Rai, S.S., K. Priestley, V.K. Gaur, S. Mitra, M.P. Singh and M. Searle (2006). Configuration of the Indian Moho beneath the NW Himalaya and Ladakh, Geophys. Res. Lett., 33, 15, 3-7, https://doi.org/10.1029/2006GL026076

Richter, C.F (1935). An instrumental earthquake magnitude scale, Bull. Seismol. Soc. Am., 25, 1, 1-32.

Sharma, M.L. (2003). Seismic Hazard in the Northern India region, Seismol. Res. Lett., 74, 2, 141-147, https://doi.org/10.1785/gssrl.74.2.141

Sharma, M.L., H.R. Wason and R. Dimri (2003). Seismic zonation of the Delhi region for bedrock ground motion, Pure Appl. Geophys., 160, 12, 2381-2398, https://doi.org/10.1007/s00024-003-2400-6

Singh, D.D. (1999). Surface wave tomography studies beneath the Indian subcontinent, J. Geodyn., 28, 2-3, 291-301, https://doi.org/10.1016/S0264-3707(98)00036-2

Singh, S.K., G. Suresh, R.S. Dattatrayam, H.P. Shukla, S. Martin, J. Havskov, X. Pérez-Campos and A. Iglesias (2013). The Delhi 1960 earthquake: Epicentre, depth and magnitude, Current Science, 105, 8, 1155-1164.

Singh, A., M. Kumar, D.D. Mohanty, C. Singh, R. Biswas and D. Srinagesh (2017). Crustal structure beneath India and Tibet: New constraints from inversion of receiver functions: Crustal structure: INDIA and TIBET. Journal of Geophysical Research: Solid Earth, 122. https://doi.org/10.1002/2017JB013946

Wessel, P., W.H.F. Smith, R. Scharroo, J. Luisx and F. Wobbe (2013). Generic Mapping Tools: Improved Version Released, EOS Trans. AGU, 94, 409-410, doi:10.1002/2013EO450001.

***CORRESPONDING AUTHOR: Deepak KUMAR**,
Department of Earthquake Engineering, Indian Institute of Technology, Roorkee-247667
e-mail: dkumar4@es.iitr.ac.in, jangradeepak80@gmail.com